Hydroxyl radicals from secondary organic aerosol decomposition in water

Haijie Tong[1], Andrea M. Arangio[1], Pascale S. J. Lakey[1], Thomas Berkemeier[1], Fobang Liu[1], Christopher J. Kampf[1,2], William H. Brune[3], Ulrich Pöschl[1] & Manabu Shiraiwa[1,*]

[1] Multiphase Chemistry Department, Max Planck Institute for Chemistry, Mainz, Germany

[2] Institute for Inorganic and Analytical Chemistry, Johannes Gutenberg University Mainz, Mainz, Germany

[3] Department of Meteorology, Pennsylvania State University, University Park, PA 16802, USA

* Correspondence to M. Shiraiwa (m.shiraiwa@mpic.de)

Abstract.

We found that ambient and laboratory-generated secondary organic aerosols (SOA) form substantial amounts of OH radicals upon interaction with liquid water, which can be explained by the decomposition of organic hydroperoxides. The molar OH yield from SOA formed by ozonolysis of terpenes (α-pinene, β-pinene, limonene) is ~0.1% upon extraction with pure water and increases to ~1.5% in the presence of Fe^{2+} ions due to Fenton-like reactions. Upon extraction of SOA samples from OH photooxidation of isoprene, we also detected OH yields of around ~0.1%, which increases upon addition of Fe^{2+}. Our findings imply that the chemical reactivity and aging of SOA particles is strongly enhanced upon interaction with water and iron. In cloud droplets under dark conditions, SOA decomposition can compete with the classical H_2O_2 Fenton reaction as the source of OH radicals. Also in the human respiratory tract, the inhalation and deposition of SOA particles may lead to a substantial release of OH radicals, which may contribute to oxidative stress and play an important role in the adverse health effects of atmospheric aerosols.

1. Introduction

Secondary organic aerosols (SOA) account for a major fraction of fine air particulate matter and have a strong influence on climate and public health (Jimenez et al., 2009; Pöschl et al., 2010; Huang et al., 2014). Formation of SOA is triggered by oxidation of volatile organic compounds followed by condensation of semi-volatile oxidation products (Hallquist et al., 2009; Donahue et al., 2012). Recently, it has been shown that extremely low volatility organic compounds (ELVOC) contribute significantly to SOA growth (Ehn et al., 2014; Jokinen et al., 2015; Mentel et al., 2015).

Particle phase chemistry and cloud processing are also efficient pathways for SOA formation and aging (Kalberer et al., 2004; Herrmann et al., 2005; Ervens et al., 2011; Shiraiwa et al., 2013). Evolution of SOA is one of the largest uncertainties in the current understanding of air quality, climate and public health (Kanakidou et al., 2005; Solomon, 2007). With regard to SOA health effects, substantial amounts of reactive oxygen species including organic radicals are detected in ambient and laboratory-generated SOA (Venkatachari and Hopke, 2008; Chen and Hopke, 2010; Chen et al., 2010; Fuller et al., 2014). Despite intensive research, multiphase chemical reactions of SOA in the atmosphere and upon interaction with the human respiratory tract are not well understood (Pöschl and Shiraiwa, 2015).

OH radicals in atmospheric droplets originate from the uptake of gaseous OH radicals (Jacob, 1986; Arakaki et al., 2013) as well as photolysis of ozone (Anglada et al., 2014). A recent study has shown that SOA can form OH radicals in the aqueous phase under light conditions (Badali et al., 2015). Under dark conditions, Fenton reactions between H_2O_2 and iron ions have been regarded as the main source of OH radicals so far (Herrmann et al., 2005). In this study, we found that OH radicals are formed by decomposition of SOA upon interactions of water and iron ions under dark conditions.

2. Methods

2.1 SOA formation and particle collection

Fig. 1 shows the experimental setup for generation of secondary organic aerosols (SOA). O_3 was used as oxidant for oxidation of α-pinene, β-pinene, limonene, and OH radicals were used for naphthalene. O_3 was generated via synthetic air (Westfalen AG, 1.8-2.1 L/min) passing through a 185

nm UV light (O_3 generator, L.O.T.-Oriel GmbH & Co. KG). The typical ozone concentrations were 600 ppb for α-pinene, β-pinene and limonene, and 1200 ppb for naphthalene. 1 mL of α-pinene (98%, Sigma Aldrich), β-pinene (99%, Sigma Aldrich) or limonene (99%, Sigma Aldrich) was kept in a 1.5 mL amber glass vial (VWR International GmbH), and 5-10 g of naphthalene crystals (99.6%, Alfa Aesar GmbH & Co. KG) were put in a 100 mL glass bottle (DURAN Group GmbH) as SOA precursor sources. 1 bar and 50-150 ccm/min N_2 (99.999%, Westfalen AG) flow was passed through these sources and the evaporated VOC vapours were introduced into a 7 L quartz flow tube reactor for gas-phase oxidation reaction with O_3 or OH radicals with a reaction time of ~3 minutes. SOA by α-pinene, β-pinene, and limonene were generated under dark and dry conditions. The flow tube reactor is surrounded by 4 UV-lights (wavelength of 254 nm, LightTech Lamp Technology Ltd.), which were turned on to generate OH radicals by photolysis of ozone and water vapour. The relative humidity in the flow tube was 30% for generating naphthalene SOA, and other experiments were conducted under dry conditions. Isoprene SOA was produced in a potential aerosol mass (PAM) chamber through the reaction of gas phase OH radicals and isoprene. The detailed information about this chamber has been described elsewhere (Kang et al., 2007; Lambe et al., 2011) and the SOA generated by the PAM chamber have been shown to be similar to SOA generated in large environmental chambers (Bruns et al., 2015; Lambe et al., 2015) and the atmosphere (Ortega et al., 2015) in terms of oxidation state and chemical composition. Briefly the isoprene vapour was taken into the chamber by N_2 gas with an estimated concentration of tens of ppm. Ozone concentration in the PAM was 6-15 ppm and relative humidity was 30-40%.

Number concentration and size distribution of the generated SOA particles were characterized using the Scanning Mobility Particle Sizer (SMPS, GRIMM Aerosol Technik GmbH & Co. KG). The typical size of the SOA ranged from 50 to 400 nm. The median diameters of the mass size distribution were 100 – 200 nm. MnO_2 (copper mesh covered with MnO_2 from ANSYCO Analytische Systeme und Componenten GmbH fixed in Gelman filter) and charcoal (4-8 mesh, Sigma Aldrich) denuders were used to remove unreacted O_3 before the collection of SOA particles on a filter. SOA was collected on 47 mm Omnipore Teflon filters (100 nm pore size, Merck Chemicals GmbH). The concentration of O_3 was monitored after an ozone denuder with an ozone analyser (typically 0-20 ppb,

model 49i, Thermo Fisher Scientific Inc.). 2 silica gel (2-4 mm, Carl Roth GmbH + Co. KG) denuders were used to dry the naphthalene SOA before collection.

Blank tests confirmed that no radicals were produced without SOA particles on a filter. Condensation of water vapour on a filter during SOA collection was negligible. A Teflon filter with particle loading was weighed using a XSE105DU balance with accuracy of ±20 μg. It was then immersed into a 0.5-1 mL 10 mM BMPO water solution and stirred with a vortex shaker (Heidolph Reax 1) for 2-7 minutes for particle extraction. A typical extraction efficiency of >70% in weight can be obtained with 7 min extraction time. After extraction, the filter was dried under 2-3 bar N_2 for ~10 minutes and the filter was weighed. The weight difference was regarded as the weight of extracted particles. The final SOA concentration depends on the extraction time and the average molar mass of SOA was assumed to be 200 g mol^{-1} in calculating SOA concentrations. The pH of SOA solutions was in the range of 4.8 - 6.4.

The Micro-Orifice Uniform Deposition Impactors (MOUDI, 110-R mode, MSP Corporation) was used for collection of ambient particles on the roof of the Max Planck Institute for Chemistry (Mainz, Germany) in 24 hour time resolution with a flow rate of 30 L/min from 17:30 PM 4th June 2015 to 17:30 PM 5th June 2015, and from 17:30 PM 7th June 2015 to 17:30 PM 8th June 2015. Particles within the diameter range of 180 – 320 nm, which is the size range dominated by organic aerosols in Mainz (Faber et al., 2013), were used for further analysis. The mass loading of these two samples on filters were ~70 and 80 μg, respectively. 47 mm diameter Teflon filters (100 nm pore size, Merck Chemicals GmbH) were used to collect the roof particles. Filters were cleaned with pure ethanol and ultra-pure water and dried by nitrogen gas before sampling and weighing. The extraction procedure is the same as that for laboratory SOA, and the field particle extracts were concentrated with a N_2 flux to obtain high signal to noise ratio spectra. Concentration of field particles in water extracts for EPR measurements were ~0.3 g L^{-1}, which is in the same order of magnitude as extracts of laboratory-generated SOA.

2.2 CW-EPR

Continuous Wave Electron Paramagnetic Resonance (CW-EPR) spectroscopy (EMXplus-10/12, Bruker, Germany) was applied for detection of radicals. 15-30 µL sample solutions were kept in a 50 µL capacity micropipette and inserted into a highly sensitive cavity (E4119001 HS-W1) for analysis. The set of EPR parameters used for this study was as follows: a modulation frequency of 100 kHz; a modulation amplitude of 0.6 or 1; microwave power of 2.149 mW (20 dB) or 21.17 mW (10 dB); a receiver gain of 40 dB; a time constant of 0.01 ms, and a magnetic field scan of 100 G. After the SOA extraction, the samples were immediately analysed by an EPR.

The spin trap 5-tert-Butoxycarbonyl-5-methyl-1-pyrroline-N-oxide (BMPO, high purity, Enzo Life Sciences GmbH) was used as a trapping agent of OH radicals. Compared to other spin trapping agents such as 5, 5-dimethyl-1-pyrroline *N*-oxide (DMPO), BMPO has the following advantages: high purity and stability in the crystalline phase; highly distinguishable EPR spectra for different structure of the trapped radicals; and spectra with high signal to noise ratio. Buffer solutions are often used in the spin trapping technique, but were not used in this study to avoid changing the real acidity environment of SOA solutions. A BMPO concentration of 10 mM was used. No significant difference was observed among 10, 20, 30, 40, and 50 mM BMPO solutions, confirming that a BMPO concentration of 10 mM is sufficient to achieve the maximum trapping efficiency. The influence of the BMPO concentration on the aqueous phase OH radical trapping efficiency for β-pinene SOA was investigated as shown in Fig. S3. Further blank tests confirmed that H_2O_2 (30%, Sigma Aldrich), Fe^{2+}, and Fe^{3+} ($Fe_2O_{12}S_3 \cdot xH_2O$, 97%, Sigma Aldrich) do not induce OH radical formation when each of them is mixed with BMPO in water (Fig. S4).

The spin counting method was applied for quantification of OH radicals using the embedded subroutine of the Bruker Xenon software (Weber, 2012). For better quantification of detected radicals, the spin fitting method (Bruker Xenon software, chapter 13 (Weber, 2012)) was used to increase the signal to noise ratio especially for low radical concentrations. The required parameters are hyperfine splitting parameters for OH radicals, which were taken from Zhao et al. (2001). Spectral simulations for radical adducts were carried out using the Matlab-based computational package Easyspin (Stoll and Schweiger, 2006). A global optimization (genetic algorithm) was conducted to obtain parameters for simulating the EPR spectrum. The parameter set was further optimized using the particle swarm

137 method within the Easyspin program. The function 'garlic' for cw EPR spectra in isotropic and fast
138 motion regimes were chosen for simulation. The hyperfine splitting constants for simulation were
139 taken from the previous work (Zhu et al., 2009).
140
141 **2.3 LC-MS/MS**
142 The SOA extracts mixed with spin trapping agent BMPO were also analysed with a
143 nanoHPLC-chip-MS/MS system (Agilent), which consists of a nano pump (G2226A) with 4-channel
144 micro-vacuum degasser (G1379B), a microfluidic chip cube with electrospray ionization (ESI) source
145 (G4240-62010) interfaced to a Q-TOF mass spectrometer (6540; nominal mass resolution 30000 at a
146 scan rate of 5 s^{-1}), a capillary pump (G1376A) with degasser (G1379B), and an auto-sampler with
147 thermostat (G1377A). All modules were controlled by Mass Hunter software (Rev. B.05.01, Agilent).
148 Eluents used were: 3% (v/v) acetone nitrile (Chromasolve, Sigma, Seelze, Germany) in water/formic
149 acid (0.1% v/v, Chromasolv, Sigma, Seelze, Germany) (Eluent A), and 3% water/formic acid (0.1%
150 v/v) in acetone nitrile (Eluent B). The flow rate was 400 nL min^{-1} with a gradient program that
151 starting with 3% B for 3 min followed by a 36 min step that raised eluent B to 60%. Further, the
152 eluent B was increased to 80% at 40 min, and returning to initial conditions within 0.1 min, followed
153 by column re-equilibration for 9.9 min before the next run. The ESI-Q-TOF instrument was operated
154 in the positive ionization mode (ESI+) with an ionization voltage of 1900 V. Fragmentation of
155 protonated ions was conducted using the auto MS/MS mode. Spectra were recorded over the mass
156 range of m/z 100-3000. Data analysis was performed using the Qualitative Data Analysis software
157 (Rev. B. 06.00, Agilent).
158
159 **2.4 Kinetic Modelling**
160 The chemical reactions used to describe the BMPO/SOA/Fe^{2+}/H_2O system, including Fenton-
161 like reactions, are listed along with their rate coefficients in Table S1. From this set of 25 reactions, 16
162 were optimized using the MCGA method and parameter ranges are given in the Table S1 to illustrate
163 the uncertainty arising from global optimization. For all other parameters reference values were taken
164 from literature, which remained fixed during optimization. Kinetic rate coefficients of a large set of

chemical reactions were determined using a uniformly sampled Monte Carlo search seeding a genetic algorithm (MCGA method (Berkemeier et al., 2013; Arangio et al., 2015)) as the global optimization method. This algorithm optimizes a kinetic model to experimental data and avoids to getting trapped in local minima during the optimization process. In the kinetic model, ROOH represents all organic hydroperoxides without resolving individual structures. This is a simplification, which is necessary for the kinetic modelling but seems to return consistent results.

3. Results and Discussion

Figure 2 indicates that EPR spectra of laboratory generated SOA by α-pinene (A), β-pinene (B), limonene (C), and isoprene (D) SOA were composed of four major peaks, whereas naphthalene SOA (E) exhibited no significant signals. These four peaks were also found for field samples (F) and became more prominent in the presence of Fe^{2+} (G). In addition, the same splitting was also observed in a solution of tert-Butyl hydroperoxide (H). Four-lines signals generated by hyperfine splittings are characteristic for BMPO-trapped OH radicals in water solution, as shown in the spectrum (I) for solutions of H_2O_2 and Fe^{2+} generating OH via the Fenton reaction ($Fe^{2+} + H_2O_2 \rightarrow Fe^{3+} + OH^- + {}^{\cdot}OH$ (Zhao et al., 2001).

Figure 3 shows LC-MS chromatograms of the BMPO-OH adduct (*m/z* 216.121) for aqueous BMPO solutions (black line) and for BMPO in aqueous β-pinene SOA extract (red line). A strong peak is observed at a retention time of 11.6 minutes for BMPO in aqueous β-pinene SOA extract, but not for the aqueous BMPO solution, which served as a blank. Confirmation of the BMPO structure for *m/z* 216.121 was achieved by comparing MS^2 spectra of $[BMPO+H^+]^+$ (*m/z* 200.126) from the aqueous standard and *m/z* 216.121. In both cases the loss of a characteristic fragment with a mass of 56.062 Da is observed (panel c and f), which corresponds to the loss of C_4H_8 from the t-butoxycarbonyl function of BMPO. Above LC-MS/MS analysis confirms the presence of OH radicals in β-pinene SOA extracts observed by EPR shown in Fig. 2.

The EPR and LC-MS/MS observations provide strong evidence that OH radicals are generated in water extracts of SOA by α-pinene, β-pinene, limonene, and isoprene as well as field fine

192 particles, which can be enhanced by Fe^{2+}. Note that additional hyperfine splitting are observed for
193 monoterpene and isoprene SOA and especially for field samples, indicating the presence of organic
194 radicals. Figure 4a shows that the amount of OH radicals trapped by BMPO increases as the SOA
195 concentration increases in the aqueous phase. The OH yield from β-pinene SOA is the highest
196 generating ~1.5 μM of OH radicals at 1.5 mM SOA concentration, followed by α-pinene, isoprene,
197 and limonene SOA. Naphthalene SOA has a negligible yield of OH radicals.

198 For assessment of potential interferences from trace amounts of impurities such as transition
199 metals in water, the OH yield was also measured in water with three different purity grades: Milli-Q
200 water (18.2 M, Thermo Scientific™ Barnstead™ GenPure™ xCAD Plus ultrapure water system),
201 TraceSELECT® Ultra ACS reagent water (Sigma Aldrich), and Savillex water (DST-1000 Acid
202 Purification System), which results in excellent agreement (Fig. 5) confirming that OH radicals can be
203 formed in the absence of transition metals.

204 Ambient particulate matter is often associated with iron ions, which play an important role in
205 aerosol chemistry via Fenton-like reactions (Deguillaume et al., 2005). To investigate the effects of
206 transition metals on OH formation by SOA, different concentrations of Fe^{2+} were added in SOA water
207 extracts. Fig. 4b-d show the OH formation efficiency (molar concentration ratio of OH and SOA:
208 [BMPO-OH]/[SOA], in %) of β-pinene, α-pinene and limonene SOA as a function of molar
209 concentration ratio of $FeSO_4$ to SOA ($[Fe^{2+}]$/[SOA]). The OH formation efficiency reaches maximum
210 values of 1.5% for β-pinene SOA, 1.1% for α-pinene SOA, and 0.5% for limonene. Different
211 behaviours in OH formation efficiency of limonene compared to α-pinene and β-pinene may be
212 induced by different organic hydroperoxide concentrations and different R subgroup structure of
213 ROOH. This order is the same as the order of the relative contribution of organic peroxides in these
214 types of SOA (Docherty et al., 2005). For isoprene SOA, the first results of ongoing experiments
215 indicate a significant increase of OH yield with increasing Fe^{2+} concentrations. The EPR spectra of
216 the isoprene SOA show a dependence on the oxidant concentration level in the PAM chamber. The
217 more complex behaviour of the isoprene SOA from OH photooxidation is under investigation and will
218 be presented in a follow-up study.

The observed formation of OH radicals is most likely due to hydrolysis and thermal decomposition of organic hydroperoxides (ROOH), which account for the predominant fraction of terpene SOA (Docherty et al., 2005; Epstein et al., 2014) as well as in rain water (Hellpointner and Gäb, 1989), but have little contribution for naphthalene SOA (Kautzman et al., 2010). ROOH are formed via multigenerational gas-phase oxidation and autoxidation, introducing multiple hydroperoxy functional groups forming extremely low volatility organic compounds (Crounse et al., 2013; Ehn et al., 2014). Due to the low binding energy of the O-O bond induced by the electron-donating R group, ROOH are well-known to undergo thermal homolytic cleavage (ROOH → RO$^{\bullet}$ + $^{\bullet}$OH, (Nam et al., 2000)). In the presence of Fe^{2+}, it has been reported that decomposition of ROOH can be enhanced mainly via Fenton-like reactions leading to heterolytic cleavage of the O-O bond in the following two ways depending on the pH and reaction environments: ROOH + Fe^{2+}→ RO$^{\bullet}$ + OH^- + Fe^{3+} or ROOH + Fe^{2+}→ RO^- + $^{\bullet}$OH + Fe^{3+} (Goldstein and Meyerstein, 1999; Deguillaume et al., 2005). Note that homolytic cleavage can be catalyzed by iron ions (Foster and Caradonna, 2003). The formed alkoxy radicals (RO$^{\bullet}$) were trapped by BMPO and found to increase as the Fe^{2+} concentration increases (Fig. 6). The formation of organic radicals in α-pinene and limonene SOA has been also detected in the previous studies (Pavlovic and Hopke, 2010; Chen et al., 2011). As shown in Fig. 4, the chemical box model including the above three ROOH decomposition pathways reproduces experimental data very well, strongly suggesting that the source of OH radicals is decomposition of ROOH. The decrease of OH radical production with increasing Fe^{2+} concentration is supposedly induced by reaction of the BMPO-OH adduct with Fe^{2+} (Yamazaki and Piette, 1990) (see also SI).

It has been suggested that hydrogen peroxide (H_2O_2) can be generated from α- and β -pinene SOA in water, but the mass yield of H_2O_2 is ~0.2% (Wang et al., 2011). In the presence of Fe^{2+}, H_2O_2 can yield OH radicals via the Fenton reaction and the formation efficiency of BMPO-OH adduct by mixtures of H_2O_2 with Fe^{2+} was measured to be ~0.6% (Fig. S2). Thus, the potential contribution of generated H_2O_2 to OH yields in β- and α-pinene SOA extracts is much lower than the observed OH radicals. Moreover, the OH yield was not affected, even if β-pinene SOA was dried under a N_2 flow

before the water extraction to evaporate particle-phase H_2O_2. Hence it is clear that the H_2O_2 in SOA should not be the dominant source of OH radicals observed in this study.

4. Implications

The implications of this finding are ellustrated in Figs. 7 and 8. The orange area in Fig. 7a shows OH production rate by Fenton reactions between Fe^{2+} and H_2O_2 forming OH radicals as a function of H_2O_2 concentration with typical dissolved iron concentrations in cloud droplets of 0.1 – 2.5 μM (Deguillaume et al., 2005). The green area shows the OH production rate by SOA decomposition in cloud or fog droplets, which ranges from ~0.01 – 100 nM s^{-1} depending on SOA precursors and the Fe^{2+} and SOA concentrations (see supplement). It clearly shows that SOA decomposition is comparably important to the Fenton reaction in most conditions and SOA can be the main source of OH radicals at low concentrations of H_2O_2 and Fe^{2+}. Water-soluble gases such as aldehydes taken up by deliquesced particles may undergo reactions in the presence of OH radicals to form low volatility products, including organic acids, peroxides, peroxyhemiacetals and oligomers (Lim et al., 2010; Ervens et al., 2011; Liu et al., 2012; Ervens, 2015; Lim and Turpin, 2015; McNeill, 2015). Thus, the formed OH radicals would promote chemical aging of SOA especially in the presence of iron ions (e.g., SOA coated mineral dust particles) (Chu et al., 2014) and may also induce aqueous-phase oxidation of sulfur dioxide forming sulfuric acid (Harris et al., 2013).

Recent studies have shown that OH radicals can trigger autoxidation reactions in the gas phase, generating highly oxidized and extremely low volatility compounds (Crounse et al., 2013; Ehn et al., 2014). In addition, it has been shown that some radicals can be long-lived in the condensed phase (Shiraiwa et al., 2011b; Gehling and Dellinger, 2013) by interacting with transition metals (Truong et al., 2010). We hypothesize that OH radicals formed from SOA decomposition could also trigger autoxidation in the condensed phase. Such a self-amplification cycle of SOA formation and aging may be relevant for example in the Amazon, where cloud and fog processing are important pathways forming a high fraction of SOA with high O:C ratio, resulting in an enhancement of cloud condensation nuclei activity of particles (Pöschl et al., 2010; Pöhlker et al., 2012). Organic peroxides are often used as the agent of the vulcanization processes to initiate the radical polymerization by

forming free radicals, which abstract hydrogen atoms from the elastomer molecules converting them into radicals that undergo oligomerization to form elastic polymer or rubber. Similar processes might also occur in SOA particles ("SOA vulcanization"), which may contribute to formation of dimers and oligomers observed in SOA particles (Kalberer et al., 2004) possibly leading to the occurrence of an amorphous solid state (Virtanen et al., 2010; Koop et al., 2011; Shiraiwa et al., 2011a; Renbaum-Wolff et al., 2013; Kidd et al., 2014).

In indoor air, terpenes are commonly found at higher concentrations than in the ambient air due to their widespread use as solvents and odorants in cleaning products and air fresheners(Weschler, 2011). Depending on precursor concentrations, the SOA concentration in indoor air can reach up to 30 μg m^{-3} with the highest contribution from limonene SOA(Waring, 2014). To evaluate potential adverse health effects by SOA deposition into the lungs, we estimated the OH production rate by SOA within the lung lining fluid (LLF) as a function of ambient SOA concentration considering breathing and deposition rates (see supplement) (Fig. 7b). The pH of lung lining fluid for healthy people is about 7.4. Our recent experiments have shown that the formation of OH radicals was increased by ~20% at a pH of 7.4 in a phosphate-buffered saline solution. Thus, the OH production rate by SOA decomposition shown in Fig. 7b may represent the lower limit. We intend to investigate pH effects on OH formation in detail in follow-up studies.

Fig. 7b also shows the OH production rate by the Fenton reaction with typical iron (Gutteridge et al., 1996) and H_2O_2 concentrations in the LLF (Corradi et al., 2008). Patients with respiratory diseases are reported to have high H_2O_2 concentrations in the bronchoalveolar lavage (Corradi et al., 2008) (as shown in shaded purple area) and the Fenton reaction may be the main source of OH radicals for such patients. However, for healthy people with low H_2O_2 and Fe^{2+} concentrations, SOA decomposition can be more important than the Fenton process under high ambient or indoor SOA concentrations. Excess concentrations of reactive oxygen species including hydrogen peroxide, OH radicals (and potentially also organic radicals) are shown to cause oxidative stress to human lung fibroblasts, alveolar cells and tissues (Pöschl and Shiraiwa, 2015). Thus, in polluted indoor or urban megacities with high SOA concentration such as in Beijing, SOA particles may play a critical role in adverse aerosol health effects.

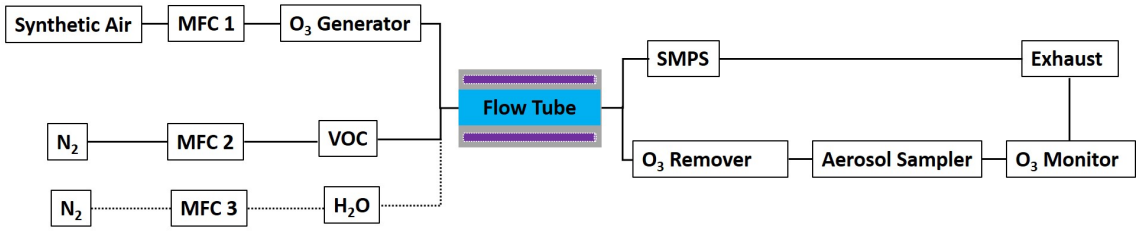

Figure 1. Schematics of the experimental setup for generation and collection of SOA particles.

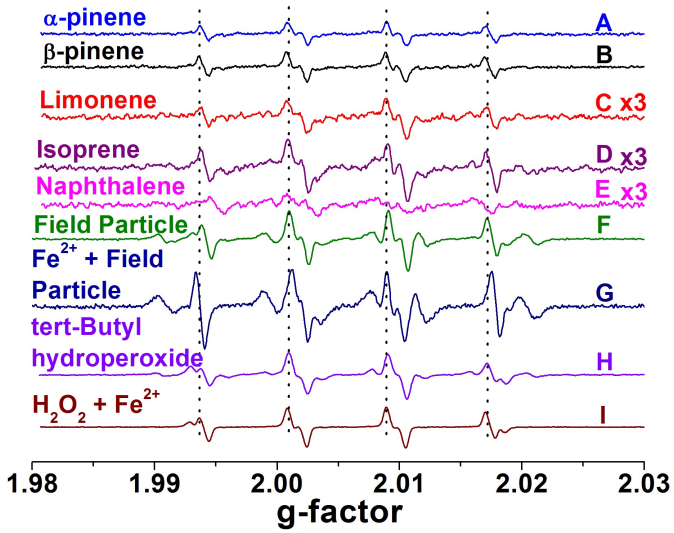

Figure 2. EPR spectra of sample solutions mixed with the spin trapping agent BMPO: (A) α-pinene SOA, (B) β-pinene SOA, (C) limonene SOA, (D) isoprene SOA, (E) naphthalene SOA, (F) 180 - 320 nm size field particles, (G) 180 - 320 nm size field particles mixed with Fe^{2+}, (H) tert-Butyl hydroperoxide solution, and (I) H_2O_2 solution with Fe^{2+}. The four peaks (dotted lines) are characteristic for BMPO-OH adducts.

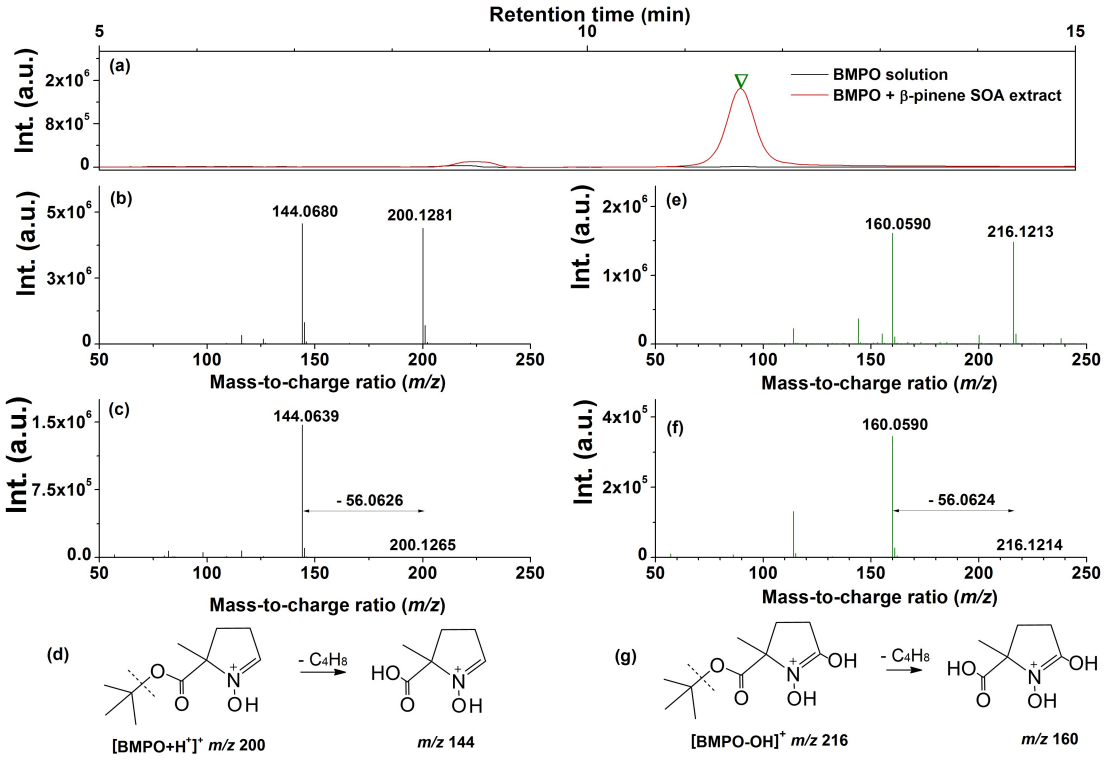

Figure 3. LC-MS/MS analysis. (a) LC-MS chromatogram of aqueous BMPO solution (black line) and BMPO mixed with β-pinene SOA water extracts (red line). The downward triangle indicates the retention time of *m/z* 216 (BMPO-OH). (b) MS spectrum of $[BMPO+H^+]^+$ with nominal *m/z* 200. (c) MS^2 spectrum of *m/z* 200, with the characteristic fragment ion *m/z* 144.0639 ($[BMPO+H^+]^+ - m/z$ 56.0626). (d) Proposed fragmentation pathway for *m/z* 200. The most abundant fragment ion present in (c) corresponds to the loss of C_4H_8 from $[BMPO+H^+]^+$. (e) MS spectrum of $[BMPO-OH]^+$ with *m/z* 216. (f) The MS^2 spectrum of *m/z* 216, with the characteristic fragment ion *m/z* 160.0590 ($[BMPO-OH]^+ - m/z$ 56.0624). (g) Proposed fragmentation pathway for *m/z* 216. The observed loss of C_4H_8 is characteristic for the fragmentation of the t-butoxycarbonyl function of BMPO.

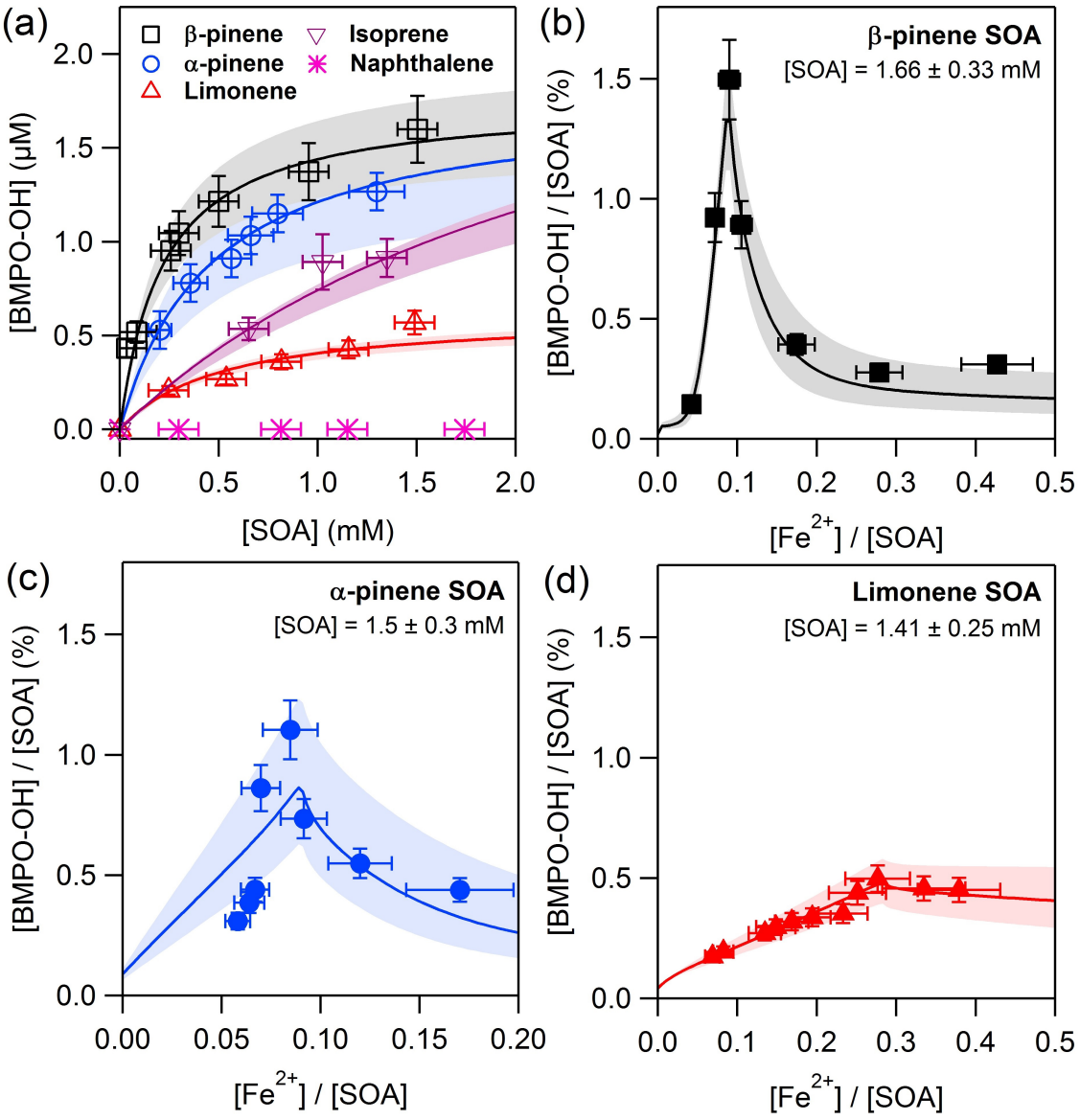

Figure 4. OH formation efficiency by SOA. (a) Concentrations of OH radicals formed in water extracts of SOA of β-pinene (black), α-pinene (blue), limonene (red), isoprene (purple), and naphthalene (pink) as a function of SOA concentrations in the aqueous phase. The formation efficiency of OH (molar concentration ratio of OH to SOA: [BMPO-OH]/[SOA], in %) in iron containing SOA water extracts against molar concentration ratios of $FeSO_4$ and SOA ($[Fe^{2+}]/[SOA]$) by (b) β-pinene, (c) α-pinene, and (d) limonene. The markers are experimental data and the solid curves with shaded area are modelled with uncertainty.

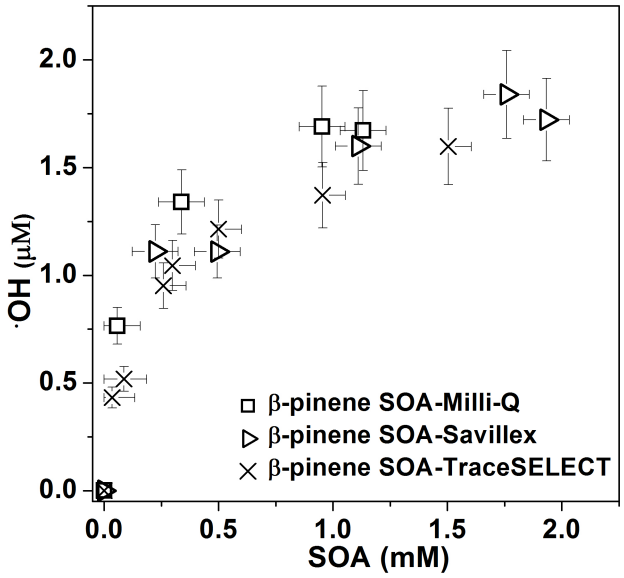

335

336 **Figure 5. OH yield of β-pinene SOA in three different kinds of pure water**: Milli-Q (squares),
337 Savillex (triangles), and TraceSELECT (Sigma, crosses).

338

339

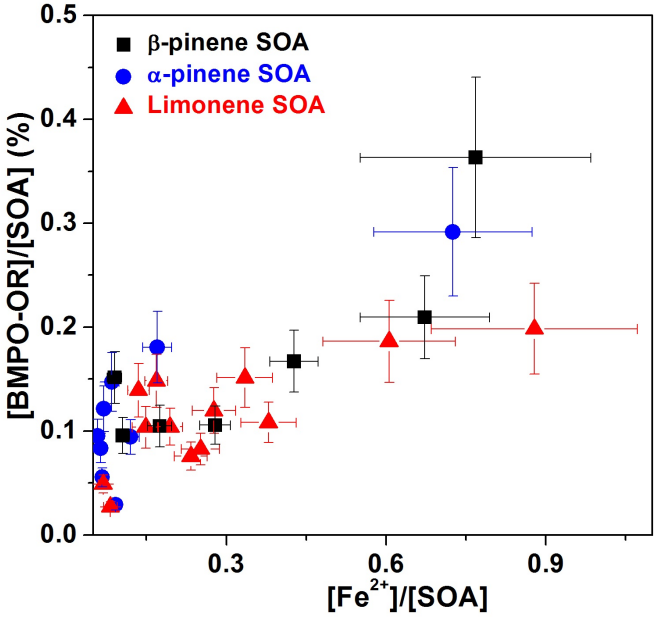

340

341 **Figure 6. Formation efficiency of organic radicals.** Molar concentration ratio of organic radicals to

342 SOA ([BMPO-OR]/[SOA], in %) in mixtures of Fe^{2+} and SOA solutions.

343

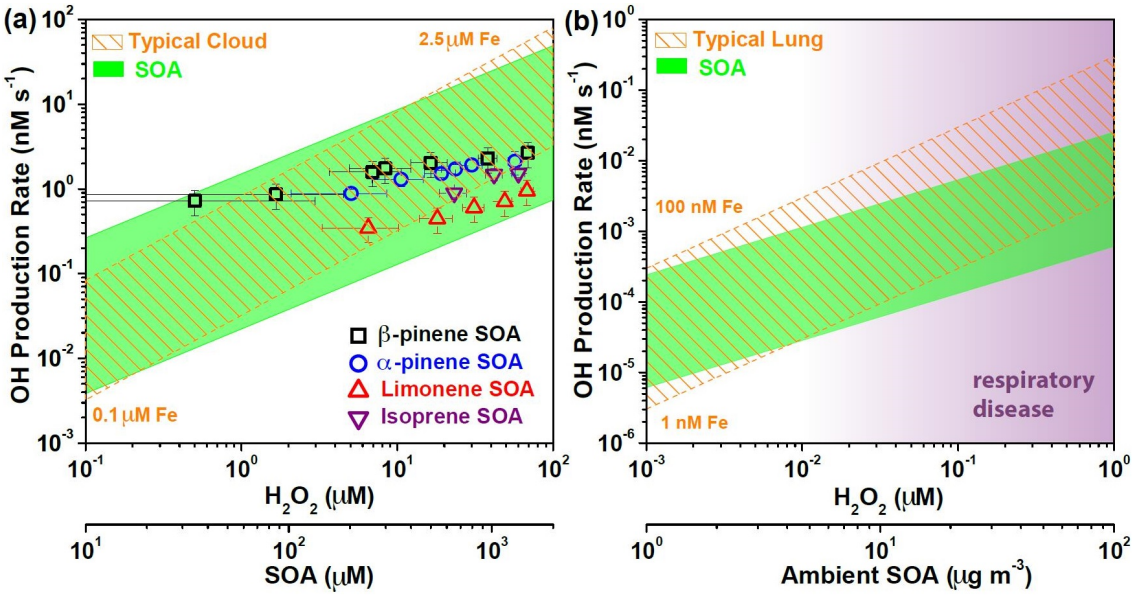

Figure 7. OH production rate in cloud droplets and lung lining fluid. (a) The OH production rate in cloud droplets by SOA decomposition compared to the classical Fenton reaction. The data points were measured in the absence of Fe^{2+} for different precursors of β-pinene (black squares), α-pinene (blue circles), limonene (red upward triangles), and isoprene (purple downward triangles). The shaded green area represents the possible range in the presence of iron as a function of SOA concentration in the aqueous phase, which is based on the minimum and maximum OH radical production efficiency of SOA in Figure 4. The dashed lines represent OH production rates due to the Fenton reaction from H_2O_2 with typical dissolved iron concentrations (Fe^{2+}:Fe^{3+} = 1:1) of 0.1 and 2.5 μM. (b) The OH production rate in lung lining fluid by SOA decomposition as a function of ambient SOA concetrations, and by the classical Fenton reaction as a function of H_2O_2 concentrations with typical dissolved iron concentrations (Fe^{2+}: Fe^{3+} = 1:1) of 100 and 1 nM. The purple shaded area represents patients with respiratory disease exhibiting high H_2O_2 concentrations in the bronchoalveolar lavage(Corradi et al., 2008).

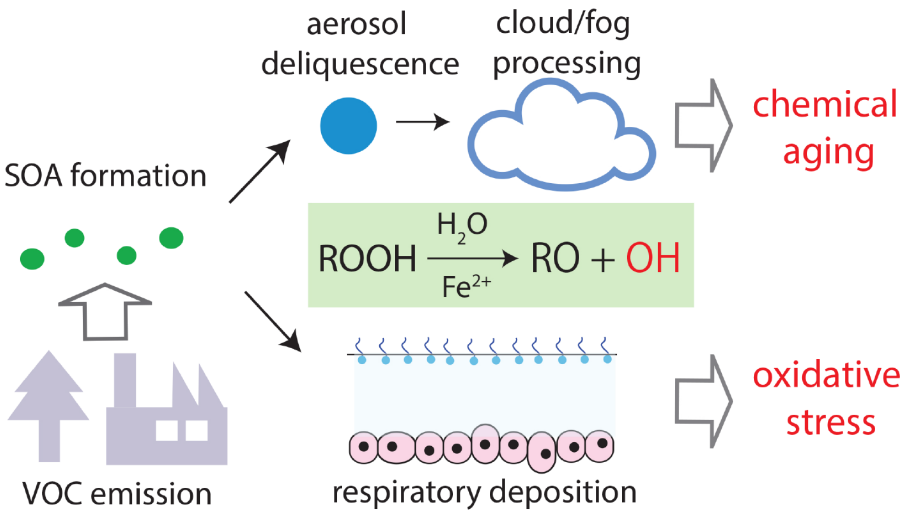

Figure 8. Implications of OH formation by SOA. Formation of OH radicals upon decomposition of organic hydroperoxides (ROOH) in secondary organic aerosol leads to rapid chemical aging of SOA particles upon deliquescence and cloud or fog processing in the atmosphere as well as oxidative stress upon inhalation and deposition in the human respiratory tract. Mixing and Fenton-like reactions of iron with ROOH from SOA can occur both in atmospheric particles and in the lung lining fluid.

Acknowledgements. This work was funded by the Max Planck Society.

References.

Anglada, J. M., Martins-Costa, M., Ruiz-López, M. F., and Francisco, J. S.: Spectroscopic signatures of ozone at the air–water interface and photochemistry implications, Proc. Natl. Acad. Sci. U.S.A., 111, 11618-11623, 2014.

Arakaki, T., Anastasio, C., Kuroki, Y., Nakajima, H., Okada, K., Kotani, Y., Handa, D., Azechi, S., Kimura, T., and Tsuhako, A.: A general scavenging rate constant for reaction of hydroxyl radical with organic carbon in atmospheric waters, Environ. Sci. Technol., 47, 8196-8203, 2013.

Arangio, A. M., Slade, J. H., Berkemeier, T., Pöschl, U., Knopf, D. A., and Shiraiwa, M.: Multiphase Chemical Kinetics of OH Radical Uptake by Molecular Organic Markers of Biomass Burning Aerosols: Humidity and Temperature Dependence, Surface Reaction, and Bulk Diffusion, J. Phys. Chem. A, 119, 4533–4544, 2015.

Badali, K., Zhou, S., Aljawhary, D., Antiñolo, M., Chen, W., Lok, A., Mungall, E., Wong, J., Zhao, R., and Abbatt, J.: Formation of hydroxyl radicals from photolysis of secondary organic aerosol material, Atmos. Chem. Phys., 15, 7831-7840, 2015.

Berkemeier, T., Huisman, A. J., Ammann, M., Shiraiwa, M., Koop, T., and Pöschl, U.: Kinetic regimes and limiting cases of gas uptake and heterogeneous reactions in atmospheric aerosols and clouds: a general classification scheme, Atmos. Chem. Phys., 13, 6663-6686, 2013.

Bruns, E. A., El Haddad, I., Keller, A., Klein, F., Kumar, N. K., Pieber, S. M., Corbin, J. C., Slowik, J. G., Brune, W. H., Baltensperger, U., and Prévôt, A. S. H.: Inter-comparison of laboratory smog chamber and flow reactor systems on organic aerosol yield and composition, Atmos. Meas. Tech., 8, 2315-2332, 2015.

Chen, X., and Hopke, P.: A chamber study of secondary organic aerosol formation by limonene ozonolysis, Indoor air, 20, 320-328, 2010.

Chen, X., Hopke, P. K., and Carter, W. P.: Secondary organic aerosol from ozonolysis of biogenic volatile organic compounds: chamber studies of particle and reactive oxygen species formation, Environ. Sci. Technol., 45, 276-282, 2010.

Chen, X., Hopke, P. K., and Carter, W. P. L.: Secondary Organic Aerosol from Ozonolysis of Biogenic Volatile Organic Compounds: Chamber Studies of Particle and Reactive Oxygen Species Formation, Environ. Sci. Technol., 45, 276-282, 2011.

Chu, B., Liu, Y., Li, J., Takekawa, H., Liggio, J., Li, S.-M., Jiang, J., Hao, J., and He, H.: Decreasing effect and mechanism of FeSO 4 seed particles on secondary organic aerosol in α-pinene photooxidation, Environ. Pollut., 193, 88-93, 2014.

Corradi, M., Pignatti, P., Brunetti, G., Goldoni, M., Caglieri, A., Nava, S., Moscato, G., and Balbi, B.: Comparison between exhaled and bronchoalveolar lavage levels of hydrogen peroxide in patients with diffuse interstitial lung diseases, Acta Biomed, 79, 73-78, 2008.

Crounse, J. D., Nielsen, L. B., Jørgensen, S., Kjaergaard, H. G., and Wennberg, P. O.: Autoxidation of organic compounds in the atmosphere, J. Phys. Chem. Lett., 4, 3513-3520, 2013.

Deguillaume, L., Leriche, M., Desboeufs, K., Mailhot, G., George, C., and Chaumerliac, N.: Transition Metals in Atmospheric Liquid Phases: Sources, Reactivity, and Sensitive Parameters, Chem. Rev., 105, 3388-3431, 2005.

Docherty, K. S., Wu, W., Lim, Y. B., and Ziemann, P. J.: Contributions of organic peroxides to secondary aerosol formed from reactions of monoterpenes with O_3, Environ. Sci. Technol., 39, 4049-4059, 2005.

Donahue, N. M., Henry, K. M., Mentel, T. F., Kiendler-Scharr, A., Spindler, C., Bohn, B., Brauers, T., Dorn, H. P., Fuchs, H., Tillmann, R., Wahner, A., Saathoff, H., Naumann, K.-H., Möhler, O., Leisner, T., Müller, L., Reinnig, M.-C., Hoffmann, T., Salo, K., Hallquist, M., Frosch, M., Bilde, M., Tritscher, T., Barmet, P., Praplan, A. P., DeCarlo, P. F., Dommen, J., Prévôt, A. S. H., and Baltensperger, U.: Aging of biogenic secondary organic aerosol via gas-phase OH radical reactions, Proc. Natl. Acad. Sci. U.S.A., 109, 13503-13508, 2012.

Ehn, M., Thornton, J. A., Kleist, E., Sipila, M., Junninen, H., Pullinen, I., Springer, M., Rubach, F., Tillmann, R., Lee, B., Lopez-Hilfiker, F., Andres, S., Acir, I.-H., Rissanen, M., Jokinen, T., Schobesberger, S., Kangasluoma, J., Kontkanen, J., Nieminen, T., Kurten, T., Nielsen, L. B., Jorgensen, S., Kjaergaard, H. G., Canagaratna, M., Dal Maso, M., Berndt, T., Petaja, T., Wahner, A., Kerminen, V.-M., Kulmala, M., Worsnop, D. R., Wildt, J., and Mentel, T. F.: A large source of low-volatility secondary organic aerosol, Nature, 506, 476-479, 2014.

Epstein, S. A., Blair, S. L., and Nizkorodov, S. A.: Direct photolysis of α-pinene ozonolysis secondary organic aerosol: effect on particle mass and peroxide content, Environ. Sci. Technol., 48, 11251-11258, 2014.

Ervens, B., Turpin, B., and Weber, R.: Secondary organic aerosol formation in cloud droplets and aqueous particles (aqSOA): a review of laboratory, field and model studies, Atmos. Chem. Phys., 11, 11069-11102, 2011.

Ervens, B.: Modeling the Processing of Aerosol and Trace Gases in Clouds and Fogs, Chem. Rev., 2015.

Faber, P., Drewnick, F., Veres, P. R., Williams, J., and Borrmann, S.: Anthropogenic sources of aerosol particles in a football stadium: Real-time characterization of emissions from cigarette smoking, cooking, hand flares, and color smoke bombs by high-resolution aerosol mass spectrometry, Atmos. Environ., 77, 1043-1051, 2013.

Foster, T. L., and Caradonna, J. P.: Fe^{2+}-catalyzed heterolytic RO-OH bond cleavage and substrate oxidation: A functional synthetic non-heme iron monooxygenase system, J. Am. Chem. Soc., 125, 3678-3679, 2003.

Fuller, S., Wragg, F., Nutter, J., and Kalberer, M.: Comparison of on-line and off-line methods to quantify reactive oxygen species (ROS) in atmospheric aerosols, Atmos. Environ., 92, 97-103, 2014.

Gehling, W., and Dellinger, B.: Environmentally Persistent Free Radicals and Their Lifetimes in PM2.5, Environ. Sci. Technol., 47, 8172-8178, 2013.

Goldstein, S., and Meyerstein, D.: Comments on the mechanism of the "Fenton-like" reaction, Acc. Chem. Res., 32, 547-550, 1999.

Gutteridge, J. M. C., Mumby, S., Quinlan, G. J., Chung, K. F., and Evans, T. W.: Pro-oxidant iron is present in human pulmonary epithelial lining fluid: implications for oxidative stress in the lung, Biochem. Biophys. Res. Commun., 220, 1024-1027, 1996.

Hallquist, M., Wenger, J. C., Baltensperger, U., Rudich, Y., Simpson, D., Claeys, M., Dommen, J., Donahue, N. M., George, C., Goldstein, A. H., Hamilton, J. F., Herrmann, H., Hoffmann, T., Iinuma, Y., Jang, M., Jenkin, M. E., Jimenez, J. L., Kiendler-Scharr, A., Maenhaut, W., McFiggans, G., Mentel, T. F., Monod, A., Prevot, A. S. H., Seinfeld, J. H., Surratt, J. D., Szmigielski, R., and Wildt, J.: The formation, properties and impact of secondary organic aerosol: current and emerging issues, Atmos. Chem. Phys., 9, 5155-5235, 2009.

Harris, E., Sinha, B., van Pinxteren, D., Tilgner, A., Fomba, K. W., Schneider, J., Roth, A., Gnauk, T., Fahlbusch, B., Mertes, S., Lee, T., Collett, J., Foley, S., Borrmann, S., Hoppe, P., and Herrmann, H.: Enhanced Role of Transition Metal Ion Catalysis During In-Cloud Oxidation of SO_2, Science, 340, 727-730, 2013.

Hellpointner, E., and Gäb, S.: Detection of methyl, hydroxymethyl and hydroxyethyl hydroperoxides in air and precipitation, Nature, 337, 631-634, 1989.

Herrmann, H., Tilgner, A., Barzaghi, P., Majdik, Z., Gligorovski, S., Poulain, L., and Monod, A.: Towards a more detailed description of tropospheric aqueous phase organic chemistry: CAPRAM 3.0, Atmos. Environ., 39, 4351-4363, 2005.

Huang, R.-J., Zhang, Y., Bozzetti, C., Ho, K.-F., Cao, J.-J., Han, Y., Daellenbach, K. R., Slowik, J. G., Platt, S. M., Canonaco, F., Zotter, P., Wolf, R., Pieber, S. M., Bruns, E. A., Crippa, M., Ciarelli, G., Piazzalunga, A., Schwikowski, M., Abbaszade, G., Schnelle-Kreis, J., Zimmermann, R., An, Z., Szidat, S., Baltensperger, U., Haddad, I. E., and Prevot, A. S. H.: High secondary aerosol contribution to particulate pollution during haze events in China, Nature, 514, 218-222, 2014.

Jacob, D. J.: Chemistry of OH in remote clouds and its role in the production of formic acid and peroxymonosulfate, J. Geophys. Res. Atmos., 91, 9807-9826, 1986.

Jimenez, J. L., Canagaratna, M. R., Donahue, N. M., Prevot, A. S. H., Zhang, Q., Kroll, J. H., DeCarlo, P. F., Allan, J. D., Coe, H., Ng, N. L., Aiken, A. C., Docherty, K. S., Ulbrich, I. M., Grieshop, A. P., Robinson, A. L., Duplissy, J., Smith, J. D., Wilson, K. R., Lanz, V. A., Hueglin, C., Sun, Y. L., Tian, J., Laaksonen, A., Raatikainen, T., Rautiainen, J., Vaattovaara, P., Ehn, M., Kulmala, M., Tomlinson, J. M., Collins, D. R., Cubison, M. J., Dunlea, E. J., Huffman, J. A., Onasch, T. B., Alfarra, M. R., Williams, P. I., Bower, K., Kondo, Y., Schneider, J., Drewnick, F., Borrmann, S., Weimer, S., Demerjian, K., Salcedo, D., Cottrell, L., Griffin, R., Takami, A., Miyoshi, T., Hatakeyama, S., Shimono, A., Sun, J. Y., Zhang, Y. M., Dzepina, K., Kimmel, J. R., Sueper, D., Jayne, J. T., Herndon, S. C., Trimborn, A. M., Williams, L. R., Wood, E. C., Middlebrook, A. M., Kolb, C. E., Baltensperger, U., and Worsnop, D. R.: Evolution of organic aerosols in the atmosphere, Science, 326, 1525-1529, 2009.

Jokinen, T., Berndt, T., Makkonen, R., Kerminen, V.-M., Junninen, H., Paasonen, P., Stratmann, F., Herrmann, H., Guenther, A. B., Worsnop, D. R., Kulmala, M., Ehn, M., and Sipilä, M.: Production of extremely low volatile organic compounds from biogenic emissions: Measured yields and atmospheric implications, Proc. Natl. Acad. Sci. U.S.A., 112, 7123-7128, 2015.

Kalberer, M., Paulsen, D., Sax, M., Steinbacher, M., Dommen, J., Prevot, A., Fisseha, R., Weingartner, E., Frankevich, V., and Zenobi, R.: Identification of polymers as major components of atmospheric organic aerosols, Science, 303, 1659-1662, 2004.

Kanakidou, M., Seinfeld, J. H., Pandis, S. N., Barnes, I., Dentener, F. J., Facchini, M. C., Van Dingenen, R., Ervens, B., Nenes, A., Nielsen, C. J., Swietlicki, E., Putaud, J. P., Balkanski, Y., Fuzzi, S., Horth, J., Moortgat, G. K., Winterhalter, R., Myhre, C. E. L., Tsigaridis, K., Vignati, E., Stephanou, E. G., and Wilson, J.: Organic aerosol and global climate modelling: a review, Atmos. Chem. Phys., 5, 1053-1123, 2005.

494 Kang, E., Root, M., Toohey, D., and Brune, W.: Introducing the concept of potential aerosol mass
495 (PAM), Atmos. Chem. Phys., 7, 5727-5744, 2007.

496 Kautzman, K. E., Surratt, J. D., Chan, M. N., Chan, A. W. H., Hersey, S. P., Chhabra, P. S., Dalleska,
497 N. F., Wennberg, P. O., Flagan, R. C., and Seinfeld, J. H.: Chemical Composition of Gas- and
498 Aerosol-Phase Products from the Photooxidation of Naphthalene, J. Phys. Chem. A, 114, 913-934,
499 2010.

500 Kidd, C., Perraud, V., Wingen, L. M., and Finlayson-Pitts, B. J.: Integrating phase and composition of
501 secondary organic aerosol from the ozonolysis of alpha-pinene, Proc. Natl. Acad. Sci. U.S.A., 111,
502 7552-7557, 2014.

503 Koop, T., Bookhold, J., Shiraiwa, M., and Pöschl, U.: Glass transition and phase state of organic
504 compounds: dependency on molecular properties and implications for secondary organic aerosols in
505 the atmosphere, Phys. Chem. Chem. Phys., 13, 19238-19255, 2011.

506 Lambe, A. T., Ahern, A. T., Williams, L. R., Slowik, J. G., Wong, J. P. S., Abbatt, J. P. D., Brune, W.
507 H., Ng, N. L., Wright, J. P., Croasdale, D. R., Worsnop, D. R., Davidovits, P., and Onasch, T. B.:
508 Characterization of aerosol photooxidation flow reactors: heterogeneous oxidation, secondary organic
509 aerosol formation and cloud condensation nuclei activity measurements, Atmos. Meas. Tech., 4, 445-
510 461, 2011.

511 Lambe, A. T., Chhabra, P. S., Onasch, T. B., Brune, W. H., Hunter, J. F., Kroll, J. H., Cummings, M.
512 J., Brogan, J. F., Parmar, Y., Worsnop, D. R., Kolb, C. E., and Davidovits, P.: Effect of oxidant
513 concentration, exposure time, and seed particles on secondary organic aerosol chemical composition
514 and yield, Atmos. Chem. Phys., 15, 3063-3075, 2015.

515 Lim, Y., Tan, Y., Perri, M., Seitzinger, S., and Turpin, B.: Aqueous chemistry and its role in
516 secondary organic aerosol (SOA) formation, Atmos. Chem. Phys., 10, 10521-10539, 2010.

517 Lim, Y., and Turpin, B.: Laboratory evidence of organic peroxide and peroxyhemiacetal formation in
518 the aqueous phase and implications for aqueous OH, Atmos. Chem. Phys., 15, 12867-12877, 2015.

519 Liu, Y., Monod, A., Tritscher, T., Praplan, A., DeCarlo, P., Temime-Roussel, B., Quivet, E.,
520 Marchand, N., Dommen, J., and Baltensperger, U.: Aqueous phase processing of secondary organic
521 aerosol from isoprene photooxidation, Atmos. Chem. Phys., 12, 5879-5895, 2012.

522 McNeill, V. F.: Aqueous organic chemistry in the atmosphere: Sources and chemical processing of
523 organic aerosols, Environ. Sci. Technol., 49, 1237-1244, 2015.

524 Mentel, T. F., Springer, M., Ehn, M., Kleist, E., Pullinen, I., Kurtén, T., Rissanen, M., Wahner, A.,
525 and Wildt, J.: Formation of highly oxidized multifunctional compounds: autoxidation of peroxy
526 radicals formed in the ozonolysis of alkenes – deduced from structure–product relationships, Atmos.
527 Chem. Phys., 15, 6745-6765, 2015.

528 Nam, W., Han, H. J., Oh, S.-Y., Lee, Y. J., Choi, M.-H., Han, S.-Y., Kim, C., Woo, S. K., and Shin,
529 W.: New insights into the mechanisms of OO bond cleavage of hydrogen peroxide and tert-alkyl
530 hydroperoxides by iron (III) porphyrin complexes, J. Am. Chem. Soc., 122, 8677-8684, 2000.

531 Ortega, A. M., Hayes, P. L., Peng, Z., Palm, B. B., Hu, W., Day, D. A., Li, R., Cubison, M. J., Brune,
532 W. H., Graus, M., Warneke, C., Gilman, J. B., Kuster, W. C., de Gouw, J. A., and Jimenez, J. L.:
533 Real-time measurements of secondary organic aerosol formation and aging from ambient air in an
534 oxidation flow reactor in the Los Angeles area, Atmos. Chem. Phys. Discuss., 15, 21907-21958, 2015.

Pavlovic, J., and Hopke, P. K.: Detection of radical species formed by the ozonolysis of α-pinene, J. Atmos. Chem., 66, 137-155, 2010.

Pöhlker, C., Wiedemann, K. T., Sinha, B., Shiraiwa, M., Gunthe, S. S., Smith, M., Su, H., Artaxo, P., Chen, Q., Cheng, Y., Elbert, W., Gilles, M. K., Kilcoyne, A. L. D., Moffet, R. C., Weigand, M., Martin, S. T., Pöschl, U., and Andreae, M. O.: Biogenic potassium salt particles as seeds for secondary organic aerosol in the Amazon, Science, 337, 1075-1078, 2012.

Pöschl, U., Martin, S. T., Sinha, B., Chen, Q., Gunthe, S. S., Huffman, J. A., Borrmann, S., Farmer, D. K., Garland, R. M., Helas, G., Jimenez, J. L., King, S. M., Manzi, A., Mikhailov, E., Pauliquevis, T., Petters, M. D., Prenni, A. J., Roldin, P., Rose, D., Schneider, J., Su, H., Zorn, S. R., Artaxo, P., and Andreae, M. O.: Rainforest Aerosols as Biogenic Nuclei of Clouds and Precipitation in the Amazon, Science, 329, 1513-1516, 2010.

Pöschl, U., and Shiraiwa, M.: Multiphase Chemistry at the Atmosphere–Biosphere Interface Influencing Climate and Public Health in the Anthropocene, Chem. Rev., 115, 4440–4475, 2015.

Renbaum-Wolff, L., Grayson, J. W., Bateman, A. P., Kuwata, K., Sellier, M., Murray, B. J., Schilling, J. E., Martin, S. T., and Bertram, A. K.: Viscosity of α-pinene secondary organic material and implications for particle growth and reactivity, Proc. Natl. Acad. Sci. U.S.A., 110, 8014-8019, 2013.

Shiraiwa, M., Ammann, M., Koop, T., and Pöschl, U.: Gas uptake and chemical aging of semisolid organic aerosol particles, Proc. Natl. Acad. Sci. U.S.A., 108, 11003-11008, 2011a.

Shiraiwa, M., Sosedova, Y., Rouvière, A., Yang, H., Zhang, Y., Abbatt, J. P., Ammann, M., and Pöschl, U.: The role of long-lived reactive oxygen intermediates in the reaction of ozone with aerosol particles, Nat. Chem., 3, 291-295, 2011b.

Shiraiwa, M., Yee, L. D., Schilling, K. A., Loza, C. L., Craven, J. S., Zuend, A., Ziemann, P. J., and Seinfeld, J. H.: Size distribution dynamics reveal particle-phase chemistry in organic aerosol formation, Proc. Natl. Acad. Sci. U.S.A, 110, 11746-11750, 2013.

Solomon, S.: Climate change 2007-the physical science basis: Working group I contribution to the fourth assessment report of the IPCC, Cambridge University Press, Cambridge, 2007.

Stoll, S., and Schweiger, A.: EasySpin, a comprehensive software package for spectral simulation and analysis in EPR, J. Magn. Reson., 178, 42-55, 2006.

Truong, H., Lomnicki, S., and Dellinger, B.: Potential for misidentification of environmentally persistent free radicals as molecular pollutants in particulate matter, Environ. Sci. Technol., 44, 1933-1939, 2010.

Venkatachari, P., and Hopke, P. K.: Development and evaluation of a particle-bound reactive oxygen species generator, J. Aerosol. Sci., 39, 168-174, 2008.

Virtanen, A., Joutsensaari, J., Koop, T., Kannosto, J., YliPirilä, P., Leskinen, J., Mäkelä, J. M., Holopainen, J. K., Pöschl, U., Kulmala, M., Worsnop, D. R., and Laaksonen, A.: An amorphous solid state of biogenic secondary organic aerosol particles, Nature, 467, 824-827, 2010.

Wang, Y., Kim, H., and Paulson, S. E.: Hydrogen peroxide generation from alpha- and beta-pinene and toluene secondary organic aerosols, Atmos. Environ., 45, 3149-3156, 2011.

Waring, M. S.: Secondary organic aerosol in residences: predicting its fraction of fine particle mass and determinants of formation strength, Indoor Air, 24, 376-389, 2014.

575 Weber, R. T.: Xenon Data Processing Reference 2012.

576 Weschler, C. J.: Chemistry in indoor environments: 20 years of research, Indoor Air, 21, 205-218,
577 2011.

578 Yamazaki, I., and Piette, L. H.: ESR spin-trapping studies on the reaction of Fe^{2+} ions with H_2O_2-
579 reactive species in oxygen toxicity in biology, J. Biol. Chem., 265, 13589-13594, 1990.

580 Zhao, H., Joseph, J., Zhang, H., Karoui, H., and Kalyanaraman, B.: Synthesis and biochemical
581 applications of a solid cyclic nitrone spin trap: a relatively superior trap for detecting superoxide
582 anions and glutathiyl radicals, Free Radic. Biol. Med., 31, 599-606, 2001.

583 Zhu, B.-Z., Shan, G.-Q., Huang, C.-H., Kalyanaraman, B., Mao, L., and Du, Y.-G.: Metal-
584 independent decomposition of hydroperoxides by halogenated quinones: Detection and identification
585 of a quinone ketoxy radical, Proc. Natl. Acad. Sci. U.S.A., 106, 11466-11471, 2009.

586

587